Thesis for The Degree of Licentiate of Engineering

Experimental Studies on the Aeroacoustics of Low-Speed Axial Fans

Michail Vourakis

Department of Mechanics and Maritime Sciences
CHALMERS UNIVERSITY OF TECHNOLOGY
Göteborg, Sweden 2023

Experimental Studies on the Aeroacoustics of Low-Speed Axial Fans
MICHAIL VOURAKIS

Licentiatavhandlingar vid Chalmers tekniska högskola
Technical report No.2023:14

Department of Mechanics and Maritime Sciences
Chalmers University of Technology
SE-412 96 Göteborg,Sweden
Telephone: +46(0)31 772 1000

Chalmers Reproservice
Gothenburg, Sweden 2023

Experimental Studies on the Aeroacoustics of Low-Speed Axial Fans
Michail Vourakis
Department of Mechanics and Maritime Sciences
Division of Fluid Dynamics
Chalmers University of Technology

Abstract

Low-speed axial fans are used in thermal management systems of internal combustion and electric vehicles. These systems are compact, cost-effective, all while addressing safety concerns. On the downside, fan operation leads to flow induced noise. Fan noise generation is strongly linked to installation effects, because they impact inflow and outflow conditions. This thesis focuses on the aeroacoustic performance of low-speed axial fans including installation effects.

An experimental study on the interplay between the aeroacoustic performance of a multi-fan system and installation conditions, is carried out. Specifically, two electric axial fans with rotating rings are installed in parallel. Inlet shroud length and distance between the fan centers are varied. It is found that the system's aerodynamic and acoustic performance is marginally affected for different fan distances. On the contrary, a longer inlet shroud improves the aerodynamic performance, while significantly amplifying the sound power over a wide frequency range. The amplification is linked to the change of radiation impedance for the fan-shroud system.

Another aspect of this work concerns the validity and improvement of acoustic measurements in a bespoke fan test facility. Initially, a round robin test of a low-pressure axial fan is conducted. Measurement repeatability of aerodynamic and acoustic performance is achieved. However, it is observed that the estimating of the fan's sound power and directivity are affected by environment effects. Consequently, a transfer function method is presented for sound power estimation. Furthermore, an approach based on spherical harmonic decomposition is outlined. This approach is poised towards source directivity studies in non-ideal acoustic environments.

Keywords: cooling fan, experimental, aeroacoustics, low-speed axial fans, low-pressure axial fans, electric fans, rotating ring, laser Doppler anemometry.

Τα καμωμένα λάθη σου μικρά είτε μεγάλα,
παθήματα-μαθήματα άμε να κάμεις κ'άλλα.
- Μ.Β.

Acknowledgments

The herein work was carried out at the Division of Fluid Dynamics, Department of Mechanics and Maritime Sciences at Chalmers University of Technology, as part of the project: eFan, a key enabler for eMobility, Part 2. The collaborators of the project are: Chalmers University of Technology, KTH Royal Institute of Technology, Volvo Group Trucks Technology and Volvo Car Corporation. Funding was provided by the Swedish Energy Agency. All measurements were performed at the facilities of Volvo Group Trucks Technology.

I would like to express my gratitude to Professor Niklas Andersson and Associate Professor Sassan Etemad for entrusting me to be part of this project and pursue my PhD studies. They have always supported me to the utmost extent and have always found the time to listen to my thoughts and give feedback, even when I do not make a lot of sense. I would also like to extend my gratitude to Doctor Mikael Karlsson, who has been a great support during the measurement campaigns, while also finding the time for interesting discussions and provide constructive feedback for improving my work. I would also like to express my gratitude to Professor Mats Åbom for being a mentor on my professional life in Sweden but also on the field of aeroacoustics. I would also like to thank Assistant Professor Elias Zea for his insightful feedback and the fruitful discussions we had, and hopefully continue to have, on acoustic signal analysis and lately spherical harmonics. There is a number of people to whom I am grateful for their support during the performed measurement campaigns. Doctor Randi Franzke and Mats Herbert who made sure the LDA measurements became feasible. Test Engineer Torbjörn Ågren who has shared his valuable experience in acoustic measurements. Engineers and Technicians at Volvo Trucks workshop, who manufactured and prepared all equipment required for the measurements. Engineer Erik Jenåker for helping with the measurements. Technicians at the Fan Test Rig for making the measurements possible and offering support at multiple occasions when problems occurred. Research Professor Valery Chernoray and Doctor Isak Jonsson for offering advice on aerodynamic measurements. Associate Professor David Sedarsky for his advice on LDA measurements. I am also thankful for the received insights and suggestions from Associate Professor Franz Zotter about spherical harmonic decomposition.

I would like to thank all my colleagues at the Division of Fluid Dynamics for creating a working environment where I feel welcome. Your success and perseverance inspire me to deal with my own challenges. Special thank you to Debarshee for showcasing invaluable support in times of need and all of you who have been good listeners in times of frustration (you know who you are).

Last but not least, I am always grateful for my friends and my family for their unwavering support and generous love.

Michail Vourakis
Göterborg, October 2023

List of Publications

This thesis is based on the following appended papers:

Paper 1. M. Vourakis, M.Karlsson. *A Round Robin Test of a Low-Pressure Axial Fan,* FAN 2022 International Conference on Fan Noise, Aerodynamics, Applications and Systems, https://doi.org/10.26083/tuprints-00021703.

Paper 2. M. Vourakis, M.Karlsson. *Aeroacoustic Interaction Effects Between Parallel Low-Pressure Axial Flow Fans,* 10th Convention of the European Acoustics Association, Forum Acusticum 2023, Torino, Italy 11-15 September 2023.

Nomenclature/Abbreviations

ICE	–	Internal Combustion Engine
EPS	–	Electric Propulsion System
TMS	–	Thermal Management System
HEX	–	Heat EXchanger
MPA	–	Micro-Perforated Absorber
FPF	–	Fan Performance Facility
SWL	–	Sound poWer Level
SPL	–	Sound Pressure Level
W	–	sound power
W_0	–	reference sound power
I	–	sound intensity
K_2	–	environment correction factor
TF	–	Transfer Function
FRF	–	Frequency Response Function
LDA	–	Laser Doppler Anemometry
BPF	–	Blade Passing Frequency
CAD	–	Computer Aided Design
PMA	–	Phased Microphone Array

Contents

Chapter 1

Introduction

1.1 Outline

The first chapter introduces the work done in the PhD project. It includes a background description, followed by a brief review of relevant published research within the field of aeroacoustics of automotive cooling fans. The chapter concludes with the main research objectives and motivation for the investigations reported in this thesis. The second chapter lists aspects of the experimental methods implemented in the appended studies. This includes information about measurement environment, relevant acoustic metrics and a transfer function method accounting for the measurement environment effects. An approach for directivity assessment within the utilized measurement environment is also outlined along with preliminary results. Moreover, information about the measurement technique used for simultaneous aerodynamic measurements is given, along with uncertainty considerations. A summary of the appended papers is given in the third chapter. Finally the last chapter summarizes the work and presents insights for upcoming studies.

1.2 Background

The latest iteration of the Global EV Outlook 2023 [1] reports exponential growth of electric car sales. New electric cars sales in 2022 have risen 5% from 2021, counting to 14% of all new cars sold in 2022. This trend is not evenly distributed around the world, as an example [1] China claims to have half of the world's electric cars. Major markets like Europe continue to adopt supportive legislation. Recently revised regulations [2] have set a 100% reduction of CO_2 emissions for new cars and vans by 2035.

The transition from ICE (Internal Combustion Engine) to EPS (Electric Propulsion System) within the automotive sector, also concerns the vehicle's noise emissions, with regards to both vehicle occupants and nearby environment [3], [4]. In particular at low speeds, e.g. road traffic within cities, the EPS powered vehicles display significant noise reduction when compared to respective ICE vehicles [3], [5]. The extent of noise reduction initially raised concerns about the safety of pedestrians, particularly for vision-impaired groups [6], [7] and subsequently led to adoption of protective legislation across the world (e.g. [8]). At higher speeds, above 50 km/h, the tyre road noise dominates total noise emissions for both EPS and ICE powered vehicles [4], [6]. Still the sound perception of occupants in a EPS powered vehicle can be different [9]. The lack of masking noise from ICE, mainly contributes to the different sound quality within EPS powered vehicles. In particular, noise sources from air-conditioning, power steering pump and TMS (Thermal Management System), are more prominent [3], [7], [10].

The TMS of a vehicle with ICE is typically comprised of a condenser, followed by a radiator and the cooling fan [11]. Similar setup is utilized for heavy duty vehicles [12], [13], although increased underhood area allows a multiple parallel fan setup or a single fan with larger diameter. Concerning EPS powered vehicles, air-cooling setups are characterised by: small volume, simple structures, high compactness and reliability, low cost and maintenance when compared to liquid or phase change material cooling setups [14].

The core component of air-cooling TMS for vehicles with ICE or EPS, is the cooling fan. The cooling fan drives the required air flow for maintaining temperatures, of critical components within ICE and EPS, at healthy operating levels. Low-speed axial fans, used in a wide spectrum of industrial applications [15], is a common choice for an air-cooling TMS. Similar to all types of cooling fans, low-speed axial fans generate flow-induced noise, commonly perceived as a byproduct of their operation. The level of the flow-induced noise from these fans, can dominate over other noise sources during certain type of vehicle operation [16]. Naturally, a substantial research focus has been placed on understanding noise mechanisms of low-speed axial fan, over the past decades.

A classification of noise mechanisms found in low-tip-speed axial fans is found in [17]. Two noise mechanisms are deemed as predominant, namely rotational and non-rotational noise. Of which the former is attributed to inflow distortion and turbulence effects, while the latter is related to blade tip clearance vortex effects. Regarding the character and operating scenarios, rotational noise is tonal and relevant at high flow coefficients, while non-rotational noise is of broadband character and important at high fan loading. The acoustic spectrum of axial fans according to Wright [18], recognizes noise sources produced by steady blade sources as unavoidable due to the required fluid work. In the same analysis, the proposed generalized acoustic spectrum notably includes, the rotor self-noise source which can be characterized by turbulent or laminar boundary layer. A later overview by Neise [19] about aeroacoustic sound generation mechanisms of fans, also implements the distinction between steady and unsteady rotating forces, both of which represent dipole type sources. The steady forces include, a uniform stationary flow mechanism of discrete character, which is considered negligible at low Mach numbers. The unsteady force mechanism has both broadband and discrete character, like secondary flows, vortex shedding and non-uniform stationary or unsteady flow.

1.3 Aeroacoustics of axial cooling fans

The understanding of both broadband and tonal character mechanisms, for low-speed axial fans, along with the models which predict their behavior, have been improving over the past decades [20]–[24]. Studying these mechanisms within the application space of vehicles TMS, has lately received increasing attention, motivated by the objectives of noise reduction and sound quality improvement.

Microphone array measurements were conducted by Amoiridis et al. [25], for evaluation of the radiator core's effect on the noise generation of an axial fan. The experimental setup comprised an automotive engine cooling module. The study, including measurements at two test facilities and various operating points, concluded that the radiator had negligible effect on sound generation and propagation. Rynell et al. [13] studied the acoustic characteristics of a heavy duty vehicle cooling module, by operating the module between an anechoic and reverberation room. Utilization of a spectral decomposition method allowed the distinction of the acoustic source from the system properties. Among the findings it was claimed that the radiator caused negligible sound attenuation. A study of sound emission effects on axial fans with upstream HEX (Heat EXchanger), was performed by Czwielong et al. [26]. They found that the HEX affects the anisotropy of the fan's inlet flow, similarly to a flow straightener. Moreover, the chosen combination of HEX geometry and fan blade skew, alter the sound emissions of the cooling module. In a subsequent study [27], it was specified that enlarged HEX surface along with round HEX geometry, could reduce total sound pressure levels of the cooling system. The main explanation behind that claim was the reduction of global turbulence levels, which were promoted by the previously mentioned HEX geometry. The effect of upstream structures on tonal noise radiation from axial fans was investigated by Park et al. [28]. Three shrouded fan configurations were tested, including the cases of no upstream component, radiator only and radiator with condenser. It was found that non-uniform inflow distributions, present in the case with upstream components, increased the respective tonal noise contributions. On the contrary, the position of radiator and condenser were linked to a reduction of broadband character noise, within a significant frequency range. The prevention of recirculating flow near the blade tip, due to the presence of the upstream structures, was reported as explanation. A study focusing on installation effects on automotive cooling fan noise was done by Lai et al. [29]. Three acoustic environments were considered, including free field, wall mounted and in-vehicle installation. It was shown that the installation effect altered the tonal sound spectra more than the broadband spectrum. Also the installation effect displayed a fan speed dependence.

The blade skew is a parameter that has received attention with regards to axial fan's aeroacoustic performance. This parameter was studied by Zenger et al. [30], under the effect of distorted inflow conditions. The distorted inflow conditions included a case of increased turbulence intensity and a case of asymmetric inflow velocity profile. Results indicated that forward-skewed fans are a better choice for undisturbed inflow conditions, while backward-skewed fans performed better for both cases of distorted inflow conditions. The blade curvature effect (i.e. forward and backward sweep) was also investigated by Henner et al. [31], within an application of an engine cooling module. The forward curvature blade fan showed better acoustic performance, interpreted as reduced density of dipole-type sources at the blade tip and lower propagation intensity. However, the backward blade fan provided better aerodynamic efficiency at the considered operating point. The blade skew was studied in combination with leading-edge serrations by Krömer et al. [32]. Different types of leading-edge serrations increased efficiency and lowered sound emissions for the tested unskewed, backward and forward skewed fans respectively. Overall the forward-skewed fan attained the best efficiency and sound reduction combination, for the majority of operating points considered. Axial fan blades with slitted leading edge, is another blade modification that was studied with regards to aerodynamic and acoustic performance by Ocker et al. [33]. A significant reduction in turbulence interaction noise was observed over a wide frequency range. However the blade modifications tested came with adverse effects on the aerodynamic performance.

Studies concerned with the noise emissions of automotive TMS, from the perspective of sound transmission path have also occurred. A combined numerical and experimental study about the effect of upstream geometry on broadband noise of automotive TMS, was performed by Piellard et al. [34]. The stationary acoustic ring, encapsulating the blade tip gap clearance, was found to alter the flow topology. Specifically a reduction of blade-tip vortice interaction and subharmonic radiation occur. This effect leads to a decrease in broadband noise in the mid-frequency range. The application of MPA (Micro-Perforated Absorber) has also been studied as means of passive noise control. A MPA shroud as well as a MPA damper, were tested for automotive cooling fans by Allam and Åbom [35]. The axial fan case displayed noise reduction in the order of 6 dB(A) for total sound power, when both MPA shroud and damper were implemented. A comprehensive study of a large scale MPA duct for an axial fan by Czwielong et al. [36], considered the parameters of fan blade skew, fan position to MPA and inflow conditions, with regards to sound emissions and performance. It was shown that the MPA duct functioned irrespective of the blade skew, while the efficiency and pressure gain was not affected when the fan was placed downstream of the duct. Moreover, the inflow turbulence did not undermine the sound reduction capability of the MPA duct, while its effectiveness concerned a wide frequency range.

Investigations of multi-fan arrangements in automotive TMS, concerning aeroustics, have not been as frequent as single fan cases. An investigation of installation effects on aeroacoustics from a four-parallel-axial-fan cluster, was performed by Karlsson and Etemad [37]. It was found that the four fan arrangement generated more noise than the individual fan setup suggested, a phenomenon which was more evident at the tonal components. This finding was attributed to a non-uniform inlet flow and high turbulence levels. A combined aerodynamic and noise performance optimization of an automotive cooling module, comprised of two parallel axial fans with different blade numbers, was performed by Guo et al. [38]. The numerical optimization space for the module included blade tip gap, distance between fans and radiators and spacing between fans. It was found that increased fan spacing can weaken the destructive interference between the two fans. Moreover, decreasing distance from radiator was associated to higher noise emissions owing to higher levels of ingested turbulence. Lastly an increase of blade tip gap was linked to back-flow effects and generation of vertices, which in turn lead to higher noise generation.

1.4 Objectives

Two principal objectives can be assigned to this work. The main objective, driving factor of this research effort, is the addition of knowledge about installation effects of low-speed axial fans from the perspective of aeroacoustics. The secondary objective concerns the establishment of experimental methods, a prerequisite for affirming the impact of carried out investigations.

Many of the experimental studies mentioned in section 1.3 [24]–[28], [30], [32], [35], [36], were carried out in anechoic facilities, representative of an acoustic free field. An important trait of acoustic free fields is that sound pressure measurements allow an explicit estimation of sound power [39]. This also holds true in reverberation rooms, however studies of source directivity are more trivial in free fields owing to the dominance of direct over reverberant sound. There are standardized methods, like ISO 3745:2012 [40], for determining sound power of comparable precision for hemi-anechoic rooms , which is an acoustic environment also broadly implemented [23], [31], [34] as representative of real world acoustic environments (e.g. a reflecting roadway). Still reflections present in hemi-anechoic rooms must be accounted for as they can undermine the measurements, for instance when assessing tonal sound [41]. The studies included in this thesis employed a bespoke testing facility which does not fit the acoustic description of the aforementioned acoustic environments. Under this light, the establishment of acoustic experimental methods, which can produce results of acceptable quality within the research field, was deemed one of the objectives.

The studies outlined in section 1.3, indicate a significant research focus on noise emissions of single low-speed axial fans, related to automotive TMS. However, only a few studies [37], [38] have been focusing on multi-fan configurations. Other studies within the context of multi-fan acoustics and installation effects, have involved centrifugal fans [42], concerned railway vehicles [43] or refrigerating units [44]. Consequently the study of a parallel axial fan system, under different installation configurations, was motivated and expressed as the main objective of this work.

Chapter 2

Aeroacoustic measurements

2.1 Measurement environment

The majority of the aeroacoustic measurements, included in this work have taken place at a FPF (Fan Performance Facility), property of Volvo Group Trucks Technology. A schematic of the FPF is depicted in Fig. 2.1. The FPF incorporates a closed loop and plenum to plenum architecture, allows control and monitoring over mass flow and pressure among other thermodynamic parameters. Thereby, it has been utilized for measuring fan performance, from a research and preliminary product evaluation perspective. More information including detailed operation of the FPF, measurement accuracy and representative research work are given by Gullberg [45].

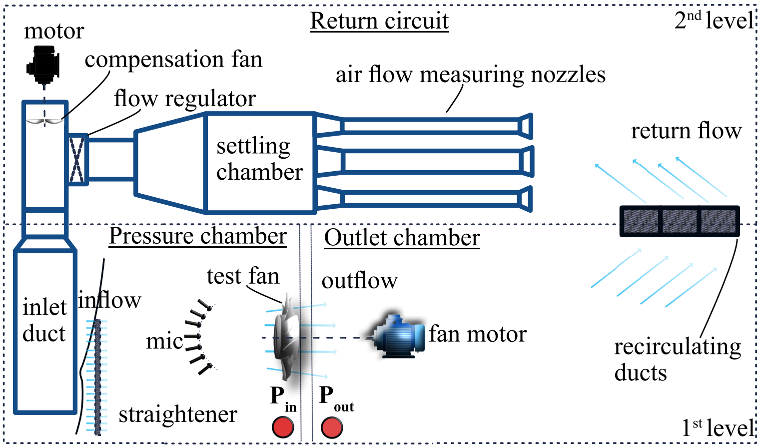

Figure 2.1: Schematic of FPF [46].

The implementation of microphone measurements, a usual case in experimental aeroacoustics, requires consideration of background noise and reflections.

Signal to noise difference below 6 dB, challenges the retrieval of aeroacoustic noise sources from interfering noise, while present reflections alter the measured sound spectra [41]. These considerations are of particular interest for this work, since the initial design of the employed FPF did not depend on them.

An approach towards diminishing measurement interference from reflections, is by transforming the acoustic properties of the measurement space towards a free field. Prior to this work, the ceiling and side walls of the FPF's pressure chamber, have been acoustically treated with the installation of standard absorption material behind a perforate grid. This acoustic treatment, dissipates reflections up to a certain wavelength, while increasing the pressure chamber's critical distance. The latter works in favor of avoiding near field effects, where hydrodynamic fluctuations of the source impact the microphone's pressure measurement. Unfortunately the current acoustic characteristics of the pressure chamber do not represent a semi anechoic room, thus a different approach is required for evaluating metrics like sound power and directivity. A different approach, which does not include modification of the environment's acoustic properties but concerns measurement technique, is the utilization of a PMA (Phased Microhone Array) [41].

The background noise levels during the operation of the FPF, originating from the compensation fan (see Fig. 2.1), do not impose great concern, when compared to the acoustic sources studied. However, there exist cases of noticeable structure borne background noise, originating from heavy machinery testing in the proximity of the FPF. This background noise concerns low frequency spectra, mainly below the lowest considered frequency for the pressure chamber, which is set at 200 Hz. Another source of unwanted background noise is flow noise emanating from the nozzles on the second floor, under choked condition. Last but not least, the fan motor has been observed to emit background noise which may infiltrate into the recorded fan sound spectra [47]. Consequently monitoring of the background noise and identification of irrelevant noise sources is deemed crucial.

2.2 Acoustic metrics

SWL (Sound poWer Level), is an acoustic metric which expresses the acoustic power radiated from a sound source. It is expressed as the logarithmic ratio of the source's emitted sound power (W) to a reference sound power (W_0). The internationally accepted value of W_0 is set to 10^{-12} *Watt* [48].

$$SWL = 10 \cdot log\frac{W}{W_0} \tag{2.1}$$

In theory SWL of a machine is independent of the acoustic environment in contrast to SPL (Sound Pressure Level), which is related to direction, distance and acoustic environment [48]. The mathematical expression (eq. (2.2) adjusted from [39]) of W, explains the insensitivity of the metric to environment influences.

$$W = \iint_S \mathbf{I} \cdot d\mathbf{S} \tag{2.2}$$

W is estimated as the surface integral of sound intensity ($\mathbf{I}$) over a surface ($\mathbf{S}$) which completely encapsulates the sound source, thereby nullifying any environment effects enclosed by the integral surface. However, interpretation of this expression in practice often involves intermediate SPL measurements, before estimating SWL or W. Thereby the estimated W, can still be exposed to environmental dependencies [39]. The reality of discrete measurement points over the surface of a sound source, only adds to the metric's inaccuracy.

Given the significance of the SWL metric in acoustics, the scientific community has produced standardized methods for its estimation, concerning different acoustic environments. ISO 3745:2012 [40] describes methods for precision level estimation of SWL in anechoic and hemi-anechoic rooms. Methods of lower accuracy, appropriate for free field over reflecting planes, are described by ISO 3744:2010 [49]. The environmental influences are considered via the calculation of an environment correction factor (K_2). Two procedures are outlined for this calculation:

- The first, denoted as absolute comparison tests, utilizes a reference sound source, usually with stable sound power output. Main assumption of this method is that the environment influence is the same for the reference sound source and the sound source of interest. This procedure is compromised if there are significant dimension differences between the two sources or if the sound source of interest has strong directivity [39].
- The second procedure is based on room absorption determination. Room absorption may be estimated based on reverberation time, utilization of two measurement surfaces over the sound source of interest and a reference sound source. Although the second procedure offers flexibility with three alternative approaches, the respective requirements for a valid estimation of K_2, are dependent on the measurement space's dimensions.

SWL does not provide information about the directionality of the sound source, a property which expresses variation of SPL at certain distance from the center of a sound source. The directivity of the sound source, is the metric which entails the previous information [50]. Knowledge of this metric aids the understanding of present noise source mechanisms which in turn facilitates noise control [41]. This metric can be illustrated by a two-dimensional polar plot of SPL or estimated as a dimensionless factor. The directivity factor ($D(\theta, \phi)$) may be defined as the ratio of mean-square sound pressure ($p_{rms}^2(\theta, \phi)$) at a given distance from the sound source's center, to the mean-square pressure (p_S^2) of an omnidirectional sound source for the same distance and SWL [51].

$$D(\theta, \phi) = \frac{p_{rms}^2(\theta, \phi)}{p_S^2} \tag{2.3}$$

Other estimator used is the directivity index, which assesses the difference between the average SPL over all angles at a given distance to the SPL at a specific angle [40], [49], [50]. Realization of this metric via acoustic measurements is ideally translated to mapping the sound field over a virtual sphere surface surrounding the sound source. However, mapping the entire surrounding surface of the sound source is often not feasible due to space limitations and flow effects [41]. Further, the possibility of a symmetric noise field deem the complete mapping as redundant [41]. Instead mapping along a streamwise plane, spanning over angle ranges in the vicinity of half circle is often implemented [25], [41]. Distribution of measurement points along this plane is suggested to $\sim 10°$ increments for many aeroacoustic investigations [41].

There exists a category of acoustic metrics concerned with the human auditory response to sound. These metrics represent the field of psychoacoustics, where assessment of sound quality is significant. Sound quality metrics include but are not limited to tonality, sharpness, roughness and loudness [51]. Naturally sound quality metrics are significant for product sound design, thus relevant to automotive applications. Subsequently automotive cooling fans, which are potentially dominating noise sources, are to be evaluated based on there metrics. At the time of this writing, measurements included in this work are being evaluated with regards to sound quality.

2.3 Transfer function method

The round robin test [47], to be discussed more in section 3.1, displayed the limitations of implementing K_2 according to ISO 3744:2010 [49] for SWL estimation in FPF's pressure chamber. To this end the herein TF (Transfer Function) method was devised, in order to provide a SWL estimation that accounts for the acoustic environment particularities of FPF's pressure chamber. This method was motivated by the reciprocity of FRF (Frequency Response Function) in linear systems. Its mathematical expression utilizes the principle of image sources [48], [50]–[52].

The Simcenter Qsources mid/high-frequency volume source was utilized for realizing the TF method. This source represents an acoustic monopole with omnidirectional characteristics. The integrated volume acceleration sensor at the nozzle of the source enables the acquisition of FRFs. The suggested frequency range for operating the source is 200-10000 Hz according to the manufacturer. The monopole source was flush mounted to the interface between the pressure and the outlet chamber of FPF (see Fig. 2.2). Measurement settings and microphone equipment utilized was as in Paper 1 [47].

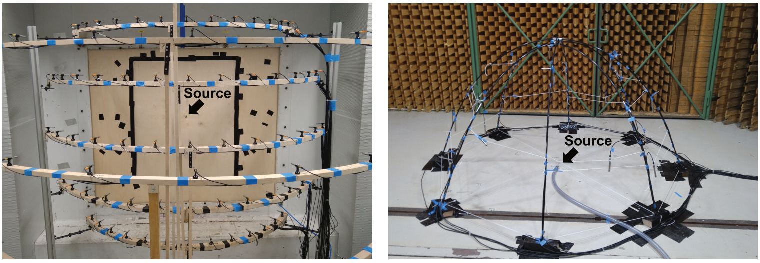

Figure 2.2: Measurement setup of monopole source at FPF (left) and semi anechoic room (right).

The measured TFs is the ratio of sound pressure at the microphone positions to the volume flow acceleration of the monopole source, given in eq. (2.4).

$$TF_{me}^{i} = \frac{P_i}{\dot{Q}} \tag{2.4}$$

Where i represents a microphone position, P_i the respective sound pressure (Pa) and $\dot{Q}$ the volume flow acceleration of the monopole source (m^3/s^2).

Each measured TF was compared with a theoretical TF of a point monopole source radiating over a hard plane surface. The theoretical TF corresponds to an ideal semi anechoic acoustic environment. Initially the free field radiation of a monopole point source is considered [48], [53]:

$$P_i = \frac{\rho j \omega Q_0}{4\pi r_i} e^{-\frac{j\omega r_i}{c}} \tag{2.5}$$

In eq. (2.5) ρ is air density (kg/m^3) and c is speed of sound (m/s) in ambient conditions, ω denotes angular frequency (rad/s), r_i is the distance (m) from the point source, and Q_0 is point source's strength, which is obtained as:

$$Q_0 = \hat{Q}_0 e^{j\omega t} \tag{2.6}$$

Where the $\hat{Q}_0$ is the volumetric flow rate (m^3/s) of the point source and t is time (s). Division of eq. (2.5) with the derivative of eq. (2.6) gives the TF of the theoretical monopole point source at distance r_i:

$$TF_{mono}^{i} = \frac{\rho}{4\pi r_i} e^{-\frac{j\omega r_i}{c}} \tag{2.7}$$

Consideration of the hard plane surface is made by utilizing the principle of image source [48], [50]–[52]. Consequently the problem translates into a free field radiation of two monopole point sources of equal source strength. This principle is illustrated in Fig. 2.3.

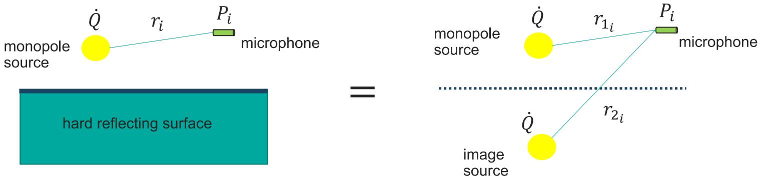

Figure 2.3: Image source principle for monopole radiation over hard reflecting surface.

Following the image source approach, the theoretical TF of a point monopole source over a hard reflecting surface is expressed as:

$$TF_{th}^{i} = \frac{\rho}{4\pi}\left(\frac{e^{-\frac{j\omega r_{2_i}}{c}}}{r_{2_i}} + \frac{e^{-\frac{j\omega r_{1_i}}{c}}}{r_{1_i}}\right) \tag{2.8}$$

Examples of theoretical TF_{th} (eq. (2.8)) are given in Fig. 2.4. In these figures measured TF_{me} (eq. (2.4)) from FPF and semi anechoic room are also included. The measurement setup for both TF_{me} is shown in Fig. 2.2.

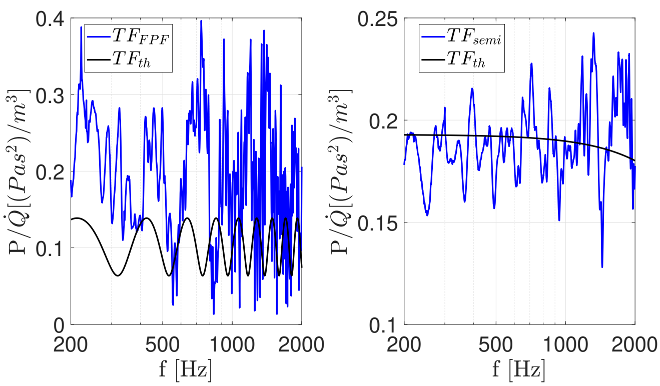

Figure 2.4: Comparison of theoretical TF_{th} and measured TF_{me} for monopole radiation: FPF (left) and semi anechoic room (right).

From the comparison of the TF, two main observations can be made. Firstly, the theoretical TF_{th} registers on average lower values than the measured TF_{FPF}. This displays the deviation of the FPF from an ideal semi anechoic environment. Apart from the hard concrete reflecting surface there is a concrete "step" and the plywood interface which separates pressure chamber from outlet chamber (see Fig. 2.2). On the contrary, the magnitude deviation between TF_{th} and TF_{semi} is smaller, since the image source principle is representing an ideal semi anechoic room. The other observation is the complexity of the TF_{me} when compared to the corresponding TF_{th}. This can be attributed to the non-ideal acoustic environment, as well as the employment of a sound source which does not accurately represent an ideal monopole point source.

The combination of the two TFs (eq. (2.8) and eq. (2.4)) enables the calculation of an environment calibration factor. This factor may be used for considering the differences of FPF from a semi anechoic room, when estimating the SWL from SPL measurements. The expression which describes the latter will then be:

$$SWL = \overline{20log\frac{P^i_{me}}{P_{ref}} - 20log\frac{TF^i_{me}}{TF^i_{th}}} + 10log\frac{S}{S_0} \tag{2.9}$$

In eq. (2.9) the bar denotes a spatial average over all microphone positions, while the last term refers to the measurement surface over the sound source. S_0 is a reference surface equal to 1 m^2. Eq. (2.9) was tested for the volume source case. The calculated SWL was compared to results according to ISO Central Secretary [49] and [40]. The two-surface method, for estimating an environment correction factor (K_2) was used when implementing ISO 3744:2010 [49]. The calculations according to ISO 3745:2010 [40] were derived from measurements in the semi anechoic room. Fig. 2.5 shows the SWL results over one-third octave. Results based on the ISO 3744:2010 method [49] show good agreement to the ISO 3745:2012 [40] results, however significant differences exist at lower and higher frequencies. One should also consider the limitation imposed by introducing K_2 in one-third octave levels. This limitation is not valid for results based on the TF method. However, the TF method under-predicts the SWL compared to the (correct) calculation made with the ISO 3745:2012 [40]. Moreover, the level of discrepancies is not constant along the considered frequency range. It could be argued that a more complicated TF_{th}, not based on the image source principle, would decrease the SWL discrepancies between TF method and ISO 3745:2012. Still application of the TF method for bigger and more complex sound sources, like a low-speed fan, would probably require the consideration of multiple monopole point sources.

2.4 Spherical harmonic decomposition approach

The inability of the transfer function to account for the environment particularities of the FPF, motivated a different approach. At the moment of this writing the validity of the methods implemented are evaluated. Therefore, only a brief description of its basics aspects will be described herein.

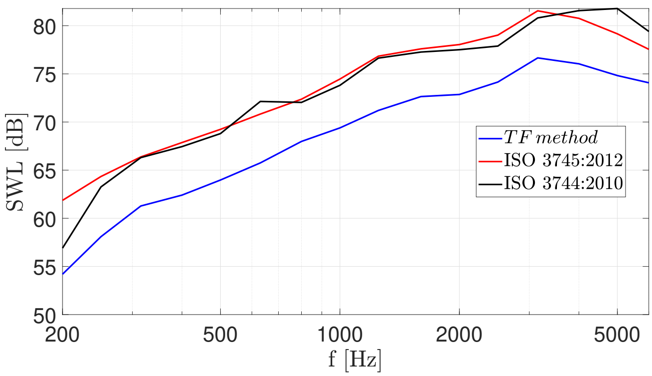

Figure 2.5: Comparison of SWL from monopole source: TF method, ISO 3744:2010 [49] with K_2 and ISO 3745:2012 [40] for semi anechoic.

The prevalence of spherical sound propagation in the far field of all sound sources, has motivated the expression of the wave equation on spherical coordinates. This expression has solutions which comprise an infinite series of spherical Bessel and Hankel functions. The first terms of this series describe sound sources with well-defined physical interpretations, like that of a pulsating sphere corresponding to a monopole [54], [55]. Moreover the directivity of these terms, when expressed as spherical wave functions, is easily expressed in spherical coordinate system. Consequently an approach utilizing the decomposition of a radiated sound field into spherical harmonics was motivated.

The scope of this approach is outlined in Fig. 2.6. A monopole radiation is recorded in the semi anechoic room as well as in the FPF. These measurements have already been performed as described in section 2.3. Subsequently decomposition of the sound field to spherical harmonics gives estimates of corresponding coefficients. These coefficients can also be used for evaluation of the relative monopole strength [56]. Assessment of coefficients and respective monopole strength from both the acoustic environments, provides a post-processing algorithm which mitigates the environment effect imposed in FPF. A successful implementation of this approach can allow directivity studies of more complicated sound sources in the FPF.

The interim steps included in the scope's outline are not trivial. To begin with one should consider that the measurement grid employed is finite. This consideration translates into an upper limit, for the order of spherical harmonic decomposition to be "correctly" estimated. A higher limit improves the accuracy of sound field reconstruction [55], especially when the radiating sound sources are complicated. For the case of the monopole source, expected in theory to be accurately reconstructed from the zero-th order spherical harmonic coefficient, there is still need to "correctly" estimate higher order terms due to the deviation from an ideal point monopole source. Another implication concerns the measurement surface covered by the measurement grid. For the

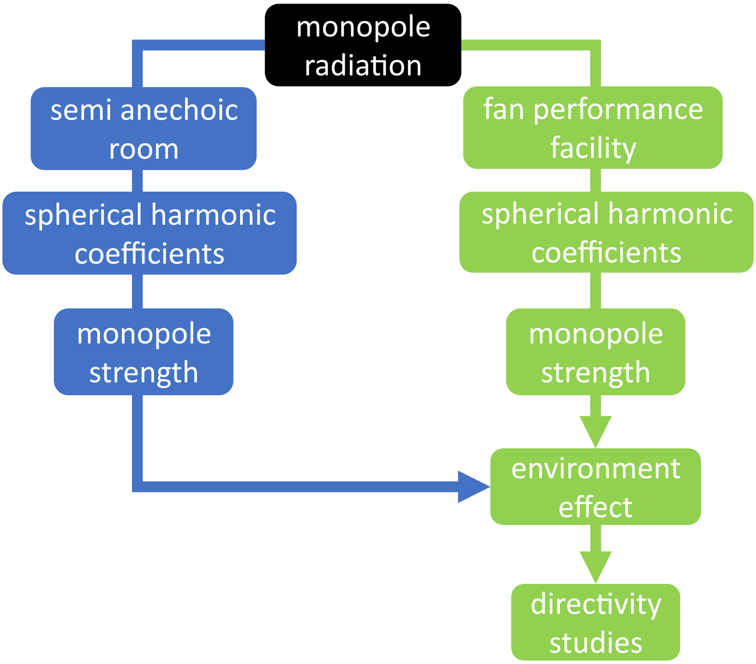

Figure 2.6: Outline of approach based in spherical harmonic decomposition.

case of the semi anechoic room measurement points are distributed over an imaginary surface of a half sphere. One can account for this by neglecting harmonics which are not represented due to physical constraints [57]. The space limitations at the FPF has led to the utilization of a measurement grid which covers a part of a spherical surface. Consequently methods which concern spherical harmonic decomposition over partial sphere surfaces [58] need to be adopted.

Overcoming the previous interim steps allows the estimation of useful acoustic parameters, including balloon plots [55] and relative monopole strength [56]. The former gives a 3D representation of the sound source's directivity, while the latter mathematically assesses the sound source's degree of isotropy. Currently the definition used in [56] has been adjusted to omit the time-harmonic dependence. The definition used is given in eq. (2.10). The parameters m and n are the degree and order of spherical harmonics, while $A_{mn}(f)$ the respective complex coefficients as calculated from the orthonormality relation of the spherical harmonic functions [57]. Preliminary results from measurements (Fig. 2.2) conducted at a semi anechoic room using the volume source in section 2.3 are given in Fig. 2.7.

$$\iota(f) = \frac{|A_{00}(f)|}{\sum_{n=0}^{\infty}\sum_{m=-n}^{n}|A_{mn}(f)|} \tag{2.10}$$

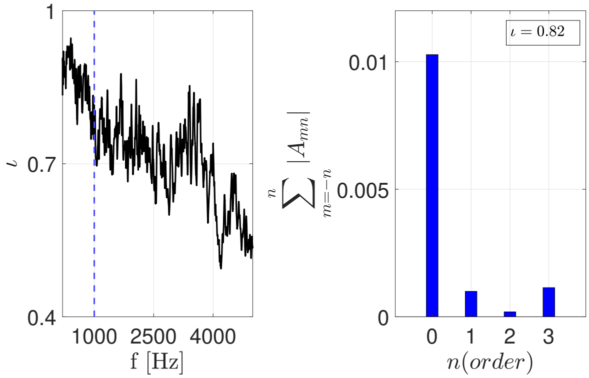

Figure 2.7: Relative monopole strength ι over frequency (left) and spherical harmonic coefficients magnitude at 1000 Hz (right).

Results have been truncated after the third order, owing to the amount of microphones installed in the measurement grid. Implementation of interpolation techniques could potentially increase the truncation limit, allowing a more comprehensive overview of the sound field. Values of ι closer to unity are indicative of an omnidirectional source, which gathers the majority of the energy in the monopole term $A_{00}(f)$. This is clearly demonstrated in the depicted results for 1 kHz. The evolution of ι over frequency demonstrates a fairly isotropic sound field up to frequencies of 4 kHz, when a significant drop is registered. There are a few more aspects in this analysis, which have been evaluated but not presented here. The first one concerns the measurement's repeatability, since data for different source positions and sound power have been acquired. Another regards the interpretation of the sound field's directivity visualised as balloon plots. Finally one can evaluate the symmetry of the energy distribution for each degree which corresponds to a specific harmonic order.

2.5 Simultaneous acoustic and aerodynamic measurements

Implementation of PMAs coupled with beamforming techniques in aeroacoustic measurements, constitutes a proven method for estimating the strength and location of sound sources [59]. This method is often characterised as non-intrusive, while it may be applied even in cases of non-acoustic hard wall wind tunnels [41], [59]. There are several successful utilizations of this method in axial fan studies [25], [33], [60]–[63]. Still as the noise mechanisms of axial fans are rooted in fluid mechanics, aerodynamic measurements are often carried out [61]–[63] in parallel for better understanding. Experimental studies without PMAs, utilize simultaneous aerodynamic measurements mainly for characterisation of the inlet flow [23], [24], [26], [27], [30], [32]. Inlet velocity profiles, turbulence intensity and integral length scales are often sought out parameters. To this end, experimental methods used can be: LDA (Laser Doppler Anemometry) [30], [32], hot-wire anemometry [26], [27], pressure probes [23] and flow visualization [24], [27].

In Paper 2 [46], acoustic measurements were complemented by velocity measurements at the fan's inlet, performed via an LDA system. In this indirect measurement technique two monochromatic laser beams intersect in the measurement volume, creating a fringe pattern. A tracer particle passing through the measurement volume, perceives two light frequencies due to the Doppler effect. The scattered light from measurement volume is then collected by a stationary detector, also invoking the Doppler effect. Superimposition of the two light waves gives rise to the Doppler frequency, which is directly proportional to the particle's flow velocity perpendicular to the bisector of the two laser beams. Identification of flow velocity's direction is acquired by shifting the frequency of one beam via a Bragg cell [64], [65].

Table 2.1: LDA measurement volume dimensions.

beam wavelength in nm	488		514.5	
focal length in mm	400	800	400	800
$dx \cdot dy \cdot dz$ in mm	$0.1131 \cdot 0.113 \cdot 2.381$	$0.1192 \cdot 0.1191 \cdot 2.51$	$0.1142 \cdot 0.1141 \cdot 2.429$	$0.1204 \cdot 0.1203 \cdot 2.561$

The LDA system used by Franzke [66] was borrowed for the velocity measurements in Paper 2 [46], albeit the LDA probe was fitted with achromatic front lenses of different focal length. This LDA system incorporates an air-cooled 300 mW argon ion laser, a fiber flow transmitter, a two-component LDA probe in backscatter mode and a BSA processor F600. The two velocity components emitted laser light with wavelengths of 514.5 and 480 nm respectively. Data processing during measurements was executed with BSA Flow software 6.72 , provided also by the LDA system manufacturer Dantec Dynamics. The particle seeding was performed by the fog generator Viper NT (Look Solutions USA), with glycol fluid (Look fluid regular-fog). The particle size is expected to be around 1 µm according to the manufacturer. The dimensions of the expected measurement volumes for the two achromatic lenses utilized are given in Table 2.1.

It should be pointed out that aerodynamic measurements and acoustic measurements included in this work [46] were acquired back-to-back. However, they are conceived as being simultaneous measurements because they were performed during the same test conditions.

2.6 Uncertainty considerations

The measurement chains employed in this work, for obtaining acoustic and aerodynamic parameters, comprise of several parts which contribute to the measurement's uncertainty. The following includes uncertainty considerations for selected parts of these measurement chains, which have not been mentioned in earlier sections.

2.6.1 Sound pressure measurements

The measurement chain concerning sound pressure measurements can be viewed as a three part system. It comprises of the measuring sensor, the equipment for data acquisition and data processing. The measuring sensors used were condenser microphones, while the data acquisition was made by a Simcenter SCADAS system. The latter also acts as a sensor power supply and signal analyzer. Data processing was handled in MATLAB.

Condenser microphones, which can be simplified as a capacitor with a moving and stationary arm, may handle unsteady pressure fluctuations in the range of 200 Pa [67]. The directly measured voltage difference is converted to an indirect sound pressure measurement, provided the known sensitivity (ratio of voltage to pressure) of the microphone. Although this is initially provided by the manufacturer, the expected material degradation over time, necessitates repetitive calibrations. Two ways of calibrating sensitivity are the reciprocity technique and the usage of sound level calibrators. The former exhibits accuracy of $\sim 0.1\ dB$ based on the method used, while the latter $\sim 0.3\ dB$ [39] over measured SPL. It should be noted that sound level calibrators calibrate at a single frequency (often chosen as 250 or 1000 Hz), thereby their usage assumes an "overall" single value sensitivity over the measuring frequency range [68]. In this work sound level calibrators were used, a choice further motivated by the practical implications of operating a measurement grids with a minimum of twenty microphones.

Microphone characteristics including type and diameter have also uncertainty implications. The free-field type used in this work is best utilized in acoustic free fields, while being pointed towards the sound source [39]. Usage in different acoustic environment is feasible when free-field corrections are applied on its frequency response [68]. These corrections also account for diffraction effects, present at frequencies corresponding to wavelengths comparable to the microphone's dimensions. Failing to consider these effects results in overestimation of sound pressure [39], [68]. Naturally smaller size microphones experience these diffraction effects at higher frequencies. To provide context, at

10 kHz the free-field correction, for random incident angle wave at a 1/2 inch microphone, is ~ 1.5 dB over obtained SPL. In this work sound spectra beyond 10 kHz, produced by investigated sound sources, did not carry significant acoustic energy.

Utilization of a finite number of microphone positions is a further cause of measurement uncertainty. For the case of SWL estimation this uncertainty (u_{mic}) can be evaluated according to ISO Central Secretary [40], [49]:

$$u_{mic} = \frac{1}{\sqrt{N_m}} \sqrt{\frac{1}{N_m - 1} \sum_{i=1}^{N_m} \left[L_{pi} - L_{pav}\right]^2} \qquad (2.11)$$

Where N_m is the number of microphone positions, L_{pi} is the SPL at microphone position i and L_{pav} the arithmetic average SPL over all microphone positions. Fig. 2.8 showcases u_{mic} for different number of microphone positions. Data from the measurements at semi anechoic room with a monopole volume source (see section 2.3) have been used.

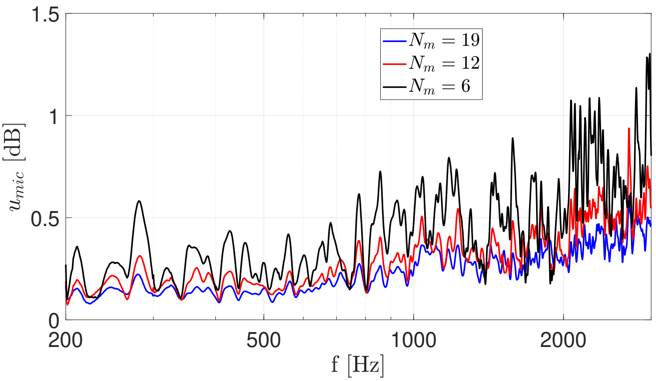

Figure 2.8: Uncertainty due to finite number of microphone positions.

As mentioned in section 2.2, estimation of SWL requires definition of a measurement surface. This surface is virtually encapsulating the sound source, with microphones being placed over the virtual surface at certain radius from the sound source. Discrepancies of radius in the order of 10 % may result in uncertainty contribution of up to 0.5 dB, according to ISO 3744:2010 [49].

Another source of uncertainty related to the data acquisition is sampling time. Longer sampling times enable segmentation of principal time to a higher number (M) of time segments. Subsequently, averaging power spectral density over a higher number of time segments according to Welch's method, induces better suppression of relative random error (ϵ_r) [69] as given by eq. (2.12):

$$\epsilon_r = \frac{1}{\sqrt{M}} \tag{2.12}$$

Where ϵ_r is expressed as the ratio of root mean square error to the signal's expected value. The effect of sampling time is further demonstrated in Fig. 2.9. Relative differences of SPL between a long ($120s$) time sample and shorter samples are shown. It should be noted that all SPL estimates utilized the same frequency resolution for the Fourier transform. The smoothing of the spectra as the sample length increases is apparent.

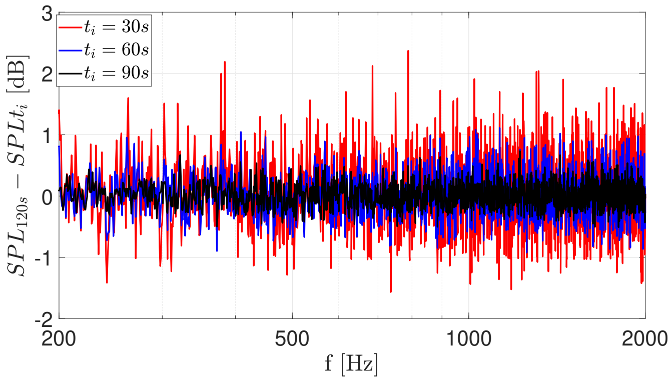

Figure 2.9: Relative difference of SPL between long and shorter sampling times.

Longer sampling time also translates into smaller frequency resolution for a given sampling rate. Consequently, a more precise estimation of spectra is feasible, although at the cost of data size and post-processing times.

Last but not least, environment conditions and their effect have to be considered when assessing measurement's uncertainty. Measurement environment's temperature and humidity affect the atmospheric sound absorption. Thereby correction of acquired sound pressure data to standard atmospheric conditions, may be performed [41]. Uncertainty evaluation of temperature and humidity variation, while estimating SWL, is given in ISO 3744:2010 [49]. The accumulated uncertainty level is below 0.5 dB, for the proposed range of measurement conditions.

2.6.2 Flow velocity measurements

As mentioned in section 2.5, seeding of flow with small particles is a prerequisite for LDA measurements. It is then no surprise that the accuracy of the measurement relies on the capability of these particles to follow the flow's fluctuations [70]. Particle size and density determine this capability [65]. In general smaller size particles may follow higher velocity gradients, however this undermines their light scattering ability which in turn compromises data acquisition. Typical particle diameters of materials eligible for air flows, range between 1 and 8 μm [71]. The attainable sampling rate is also strongly related to particle size and density. This is easier to grasp if one considers measurement dropout. Dropout describes the interruption of data acquisition while no particles cross the measurement volume [70]. Equation (2.13) gives the dropout percentage for gas flows.

$$DO = 100\left(1 - \eta\frac{\rho_g}{\rho_p}\frac{V_m}{V_p}\right) \tag{2.13}$$

Where V_m and V_p stand for the volume of measurement region and particle respectively, ρ_g and ρ_p are densities of gas and particle respectively, while η denotes ratio of particle to gas mass flow. The glycol material used in Paper 2 [46] was released in the flow as fog through a vaporizer. The particle size distribution from this method was not very narrow (0.2-10 μm), according to the manufacturer. This distribution coupled with measurement conditions (temperature, pressure and humidity) which affected the evaporation of the fog, led to high dropout percentages. Consequently measurement times were prolonged in order to increase measured samples.

Deciding measurement time while utilizing LDA, is also depended on the presence of the velocity bias effect. This effect concerns the dependency of velocity sampling rate in LDA measurements, on the velocity magnitude. In particular the sampling of high velocity particles will be more frequent than low velocity ones [65], thus estimators of statistical moments including mean flow velocity, will be biased.

One way of avoiding the velocity bias is by obtaining statistically independent samples. Statistically independent samples are obtained when the temporal distance between consecutive samples, is greater than two times the flow's integral time scale (T_u) [64], [71]. A good approximation of T_u is the ratio of macro-length scale (L_u) of the problem to the mean velocity ($\bar{u}$), as given in equation (2.14) retrieved from [64].

$$T_u = \frac{L_u}{\bar{u}} \tag{2.14}$$

A more precise estimation of T_u can be based on the autocovariance ($C_{uu}(\tau)$) of the measured velocity time signal, given in equation (2.15) adjusted from [71].

$$T_u = \int_0^{\infty} \frac{C_{uu}(\tau)}{C_{uu}(0)}\, d\tau = \int_0^{\infty} \rho_{uu}(\tau)\, d\tau \tag{2.15}$$

Where τ stands for the time lag considered when calculating autocovariance. The parameter $\rho_{uu}(\tau)$ showcases a rapid decay towards zero, after which it stabilizes. The first crossing of $\rho_{uu}(\tau)$ is usually considered as the upper integration limit [71] of equation (2.15). A typical estimation of $\rho_{uu}(\tau)$ is given in Fig. 2.10. The estimation was made for data taken from Paper 2 [46]. It should be noted that estimation of T_u has to be made across all positions of the measurement grid. Subsequently the maximum T_u will dictate the allowable temporal distance for independent consecutive samples [71].

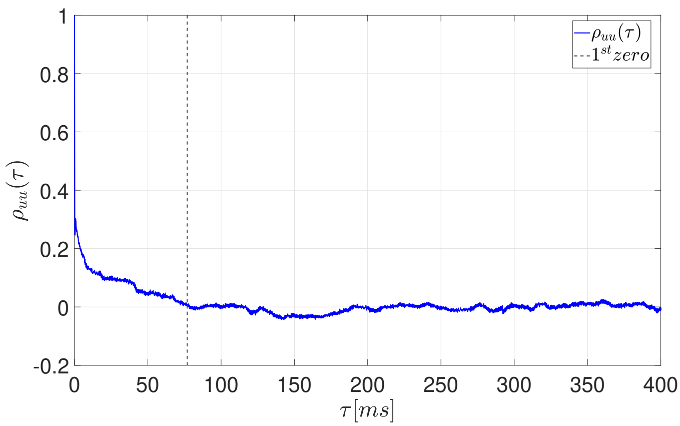

Figure 2.10: Representative estimate of $\rho_{uu}(\tau)$ upstream of low-speed axial fan.

Another way of treating the velocity bias is by using the transit time [64], [65], [71] which corresponds to each measured seeding particle. The transit time (t_i) of a measured particle, refers to its corresponding signal duration while crossing the measurement volume [64]. This time information can be used for estimating a weighting factor (η_i) for each measured particle, as shown in equation (2.16) adjusted from [71]. Subsequently η_i is utilized as a multiplication factor for estimating statistical moments of the flow.

$$\eta_i = \frac{t_i}{\sum_{j=0}^{N-1} t_j} \tag{2.16}$$

The small dimensions of the measurement volume, typically 0.1 mm thickness and 0.3-3 mm length, motivate the assumption of uniform flow across it [65]. Having already accounted for the velocity bias, there is no need for further weighting of measured samples prior to estimating mean velocities and higher moments. However the assumption of uniform flow may be irrelevant if a non-uniform fringe spacing is characterising the measurement volume.

Non-uniform fringe spacing may arise from improper optical layout, astigmatism and laser light diffraction via particles intersecting the laser beams [65]. Failing to discover it may result in estimators of mean velocity and turbulence intensity contaminated with systematic errors [64], [65]. The systematic error is generally more important for flow turbulence than mean flow velocity. An over-estimation of turbulence intensity is expected due to fringe distortion, which is less significant the higher the turbulence intensity of the flow is [65].

Finally, a practical consideration which concerns the measurement volume and affects measurement accuracy, is the alignment of the measurement volume in relation to the investigated flow field. This consideration is particularly important when multiple lenses are utilized in conjunction with the LDA probe. As noted in section 2.5 lenses of different focal lengths have been used along with two different setups, in Paper 2 [46]. This was done for obtaining all three velocity components along the velocity profile of interest. Since a two-component LDA system was used, one of the velocity components (tangential) was obtained twice. Although the agreement between the mean tangential velocity profiles was reasonable (fig. 9 in Paper 2 [46]), the level of discrepancies motivate longer measurement times for a sufficiently accurate estimator of the flow field's turbulence intensity.

Chapter 3

Summary of Papers

3.1 Paper 1

In Paper 1, a round robin test for a low-pressure axial fan was performed in order to assess the attainable measurement quality at the available testing facility. The aim was to reproduce part of acoustic and aerodynamic results from a benchmark fan case study [72], while evaluating measurement repeatability.

3.1.1 Methodology

Three copies of the benchmark fan along with one copy of stator, inlet and outlet shroud were 3D-printed via laser sintering. Sanding and filling with paint was used to improve roughness and assebly of the 3D-printed parts. The final version was compared to the reference fan design via 3D scanning. Characteristic curves (pressure rise and efficiency over mass flow) of the three fan copies were obtained at the FPF across a wide operation range. In addition acoustic measurements were performed for the estimation of the sound characteristic curve along with the directivity of the fan setup. The acoustic measurements were performed upstream of the fan's inlet via free-field microphones distributed over two spherical surfaces of different radii. The estimation of SWL was made by utilizing ISO 3744:2010 [49] with a K_2 according to the reverberation method. SWL was assessed at a narrow band and one-third octave basis.

3.1.2 Discussion

The repeatability of the measurements was perceived as satisfactory. The pressure rise curves of the three tested fans showcased discrepancies within the expected measurement accuracy across the operation map. The efficiency curves did not register same degree of repeatability across the operation range, mainly attributed to the low accuracy of the torque sensor. The sound characteristic curves of the fans showed good repeatability with discrepancies of highest magnitude registered at highest mass flows. The narrow band spectra of SWL at the design point showed good agreement for the three fans and the frequency range considered. The reproducibility of the attained results with regards to Zenger et al. [72] was deemed improvable. The pressure rise curve was quantitatively reproduced for the majority of the operating points, though considerable discrepancies were found at high flow rates. The efficiency curve was reproduced qualitatively, showcasing a relative stable discrepancy to the measured curves. The sound characteristic curve was reproduced well at the design point onward, as well as flow rates corresponding to deep stall. However, big discrepancies were registered at the remainder of the measured operation points. Comparison of the narrow band spectra at the design point revealed a phase mismatch at the lowest frequencies, until second BPF (Blade Passing Frequency), along with magnitude discrepancies. This behavior was mainly attributed to dimensional imperfections during the assembly of the fan setup, rooted in geometrical discrepancies from the CAD (Computer Aided Design) model. Namely a maximum 2° bending of the fan's blade compared to the model and an asymmetric shroud-to tip clearance. Finally the evaluation of directivity showed retainment of the sound field's symmetry, along the polar angle range measured.

3.2 Paper 2

In Paper 2, an aeroacoustic investigation of parallel low pressure axial fans under varied installation conditions was performed. The aim was to expose any interaction effects within the range of tested installation conditions, which could hamper the overall acoustic or aerodynamic performance of the system.

3.2.1 Methodology

A low-speed/pressure electric axial fan with a rotating ring was utilized for the study. The parallel fan installation was tested for different distances between the fans and different lengths of the inlet shrouds. A single fan case was also tested as reference, for all inlet shroud lengths. The FPF was utilized for acoustic and aerodynamic measurements at selected operating points. Acoustic measurements were performed upstream of the fan system's inlet, over spherical surface segments corresponding to two radii. SWL estimation was made by utilizing ISO 3744:2010 [49] with a K_2 according to the two surface method. Moreover, aerodynamic measurements were performed, in proximity to the fan's aerodynamic interface plane, for one case of inlet shroud length. The aerodynamic measurements utilized LDA, allowing the estimation of velocity profiles as well as investigation of corresponding power spectral density.

3.2.2 Discussion

Overall aerodynamic and acoustic performance of the fan system showcased insensitivity to the variation of the distance between fans. The inlet velocity profiles attained showcased an increasing asymmetry as the distance between fans decreased. However, these effects did not translate to noticeable discrepancies when examining the characteristic curve or the sound spectra of the system. The inlet shroud length constituted alterations to both aerodynamic and acoustic performance of the system. The fan system and the single fan reference case, registered gains along their characteristic curves while showcasing more predictable stall region, when fitted with the longer inlet shroud. On the contrary, the longer inlet shroud increased the SWL across the lower frequencies substantially while attenuating levels slightly at higher frequencies. Moreover, low-frequency spectra of broadband character showcased broadening over frequency. This behavior has been attributed to the alteration of the fan/shroud radiation impedance with the introduction of the longer inlet shroud. Finally the spectral density analysis of the inlet velocity profiles, showcased the persistence of energy at frequencies corresponding to the first motor orders.

Chapter 4

Concluding remarks

4.1 Summary

A series of experimental aeroacoustic studies, concerning installation effects on low-speed/pressure axial fans has been done. The aim of these studies has been twofold. One part concerned the establishment of experimental methods while another focused on investigating multi-fan arrangements.

The establishment of experimental methods has been initiated with a round robin test, summarized in 3.1. This test verified the applicability of the FPF for attaining steady and repeatable operating conditions for investigated fan setups and showcased the potential for acoustic measurements. A transfer function method for improving SWL estimation from acoustic measurements at the FPF was described in section 2.3. However, the attained results when compared to established methodologies like ISO 3744:2010 [49], did not suggest further investment. Consequently, a new approach based on spherical harmonic decomposition, was outlined in section 2.4. Preliminary results hint at a positive direction, towards directivity characterization of sound sources at the FPF.

The experimental study on multi-fan arrangements investigated dependencies between aeroacoustic and installation parameters. The multi-fan system's performance showcased weak coupling with regards to the distance between the fans. Obtained velocity profiles at fan's inlet demonstrated increased asymmetry as the distance between fans decreased. Still this behavior did not translate into performance penalties from an acoustic or aerodynamic perspective. On the contrary, elongation of the inlet shrouds proved detrimental to the acoustic performance, while providing modest aerodynamic gains. Specifically, SWL of both tonal and broadband character were drastically increased at lower frequencies, whilst marginally decreased at higher frequencies. Higher pressure rise and stability at the stall region, portrayed the aerodynamic gains.

4.2 Future work

The approach described in section 2.4 has the potential to provide a method for directivity studies in a non-ideal acoustic environment. Subsequently installation effects on fan noise directivity under different operating conditions can be investigated. These investigations can be complemented, by documenting relative changes of SWL, as well as flow field information. The flow field information may include velocity profiles and turbulence levels at the fan's inlet plane and/or along the blade path. Thereby, the identification of present fan noise mechanisms can be achieved. An alternative measurement approach is via utilization of PMAs. As mentioned in section 2.5, a microphone array may provide simultaneous quantification and localization of fan noise sources. However, the successful implementation of a PMA in a hard walled environment requires significant suppression of inherent image sound sources. This requirement will dictate the choice of beamforming algorithm and positioning of the array in relation to the sound source [41].

As showcased in Paper 2, the investigated multi-fan system experienced a notable modification of its acoustic identity in conjunction with inlet shroud length. Thus, quantification of such modifications with regards to sound quality metrics is recommended. Study cases could comprise of different axial fan designs and/or levels of complexity concerning installation geometry.

Bibliography

[1] *IEA 2023, Global EV Outlook 2023, IEA, Paris 2023, License: CC BY 4.0*, 2023 (cit. on p. 1).

[2] *Fit for 55: Council adopts regulation on CO2 emissions for new cars and vans, Council of the European Union*, 2023 (cit. on p. 1).

[3] G. Cerrato, “Automotive sound quality-powertrain, road and wind noise”, *Sound and Vibration*, vol. 43, no. 4, 16 – 24, 2009 (cit. on pp. 1, 2).

[4] L. M. Iversen, G. Marbjerg and H. Bendtsen, “Noise from electric vehicles-’state of the art’literature survey”, in *INTER-NOISE and NOISE-CON Congress and Conference Proceedings*, Institute of Noise Control Engineering, vol. 247, 2013, pp. 267–271 (cit. on pp. 1, 2).

[5] J. Jabben, E. Verheijen and C. Potma, “Noise reduction by electric vehicles in the netherlands”, in *Inter-Noise and Noise-Con Congress and Conference Proceedings*, Institute of Noise Control Engineering, vol. 2012, 2012, pp. 6958–6965 (cit. on p. 2).

[6] E. Verheijen and J. Jabben, “Effect of electric cars on traffic noise and safety”, 2010 (cit. on p. 2).

[7] K. Genuit and A. Fiebig, “Sound design of electric vehicles-challenges and risks”, in *INTER-NOISE and NOISE-CON Congress and Conference Proceedings*, Institute of Noise Control Engineering, vol. 249, 2014, pp. 3492–3501 (cit. on p. 2).

[8] *Regulation no 138 of the economic commission for europe of the united nations (unece) — uniform provisions concerning the approval of quiet road transport vehicles with regard to their reduced audibility [2017/71]*, 2017 (cit. on p. 2).

[9] H. Huang, X. Huang, W. Ding, M. Yang, D. Fan and J. Pang, “Uncertainty optimization of pure electric vehicle interior tire/road noise comfort based on data-driven”, *Mechanical Systems and Signal Processing*, vol. 165, p. 108 300, 2022 (cit. on p. 2).

[10] N. C. Otto, R. Simpson and J. Wiederhold, “Electric vehicle sound quality”, SAE Technical Paper, Tech. Rep., 1999 (cit. on p. 2).

[11] J. D. Walter, “Automotive cooling system component interactions”, Ph.D. dissertation, Texas Tech University, 2001 (cit. on p. 2).

[12] S. Etemad and P. Gullberg, "Validation of urans simulation of truck cooling fan performance", in *ASME International Mechanical Engineering Congress and Exposition*, American Society of Mechanical Engineers, vol. 46545, 2014, V007T09A048 (cit. on p. 2).

[13] A. Rynell, G. Efraimsson, M. Chevalier and M. Abom, "Acoustic characteristics of a heavy duty vehicle cooling module", *Applied acoustics*, vol. 111, pp. 67–76, 2016 (cit. on pp. 2, 3).

[14] G. Zhao, X. Wang, M. Negnevitsky and H. Zhang, "A review of air-cooling battery thermal management systems for electric and hybrid electric vehicles", *Journal of Power Sources*, vol. 501, p. 230 001, 2021 (cit. on p. 2).

[15] S. Castegnaro, "Aerodynamic design of low-speed axial-flow fans: A historical overview", *Designs*, vol. 2, no. 3, p. 20, 2018 (cit. on p. 2).

[16] R. C. Chanaud and D. Muster, "Aerodynamic noise from motor vehicles", *The Journal of the Acoustical Society of America*, vol. 58, no. 1, pp. 31–38, 1975 (cit. on p. 2).

[17] R. E. Longhouse, "Noise mechanism separation and design considerations for low tip-speed, axial-flow fans", *Journal of Sound and Vibration*, vol. 48, no. 4, pp. 461–474, 1976 (cit. on p. 2).

[18] S. Wright, "The acoustic spectrum of axial flow machines", *Journal of Sound and Vibration*, vol. 45, no. 2, pp. 165–223, 1976 (cit. on p. 2).

[19] W. Neise, "Review of fan noise generation mechanisms and control methods", in *International Symposium on Fan Noise 1.-3.9.1992 Seulis, France*, LIDO-Berichtsjahr=1992, Publications CETIM, Seulis, France, 1992, pp. 45–56. [Online]. Available: `https://elib.dlr.de/36932/` (cit. on p. 2).

[20] S. Moreau and M. Roger, "Competing broadband noise mechanisms in low-speed axial fans", *AIAA journal*, vol. 45, no. 1, pp. 48–57, 2007 (cit. on p. 3).

[21] S. Moreau and M. Sanjose, "Sub-harmonic broadband humps and tip noise in low-speed ring fans", *The Journal of the Acoustical Society of America*, vol. 139, no. 1, pp. 118–127, 2016 (cit. on p. 3).

[22] S. Magne, S. Moreau and A. Berry, "Subharmonic tonal noise from backflow vortices radiated by a low-speed ring fan in uniform inlet flow", *The Journal of the Acoustical Society of America*, vol. 137, no. 1, pp. 228–237, 2015 (cit. on p. 3).

[23] E. Canepa, A. Cattanei, F. M. Zecchin, G. Milanese and D. Parodi, "An experimental investigation on the tip leakage noise in axial-flow fans with rotating shroud", *Journal of Sound and Vibration*, vol. 375, pp. 115–131, 2016 (cit. on pp. 3, 5, 17).

[24] M. Sturm and T. Carolus, "Tonal fan noise of an isolated axial fan rotor due to inhomogeneous coherent structures at the intake", *Noise Control Engineering Journal*, vol. 60, no. 6, pp. 699–706, 2012 (cit. on pp. 3, 5, 17).

[25] O Amoiridis, A Zarri, R Zamponi *et al.*, “Sound localization and quantification analysis of an automotive engine cooling module”, *Journal of Sound and Vibration*, vol. 517, p. 116 534, 2022 (cit. on pp. 3, 5, 10, 16).

[26] F. Czwielong, F. Krömer and S. Becker, “Experimental investigations of the sound emission of axial fans under the influence of suction-side heat exchangers”, in *25th AIAA/CEAS aeroacoustics conference*, 2019, p. 2618 (cit. on pp. 3, 5, 17).

[27] F. Czwielong, J. Soldat and S. Becker, “On the interactions of the induced flow field of heat exchangers with axial fans”, *Experimental Thermal and Fluid Science*, vol. 139, p. 110 697, 2022 (cit. on pp. 3, 5, 17).

[28] M. Park, D.-J. Lee and H. Lee, “Inflow effects on tonal noise of axial fan under system resistances”, *Applied Acoustics*, vol. 192, p. 108 737, 2022 (cit. on pp. 3, 5).

[29] Y. Lai, C. Weng, Y.-Y. Lu, M. Karlsson, M. Abom and M. Knutsson, “Study of installation effects on automotive cooling fan noise”, *SAE International Journal of Advances and Current Practices in Mobility*, vol. 5, no. 2022-01-0935, pp. 803–809, 2022 (cit. on p. 3).

[30] F. J. Zenger, A. Renz, M. Becher and S. Becker, “Experimental investigation of the noise emission of axial fans under distorted inflow conditions”, *Journal of Sound and Vibration*, vol. 383, pp. 124–145, 2016 (cit. on pp. 4, 5, 17).

[31] M. Henner, B. Demory, M. Alaoui, M. Laurent and B. Behey, “Effect of blade curvature on fan integration in engine cooling module”, in *Acoustics*, MDPI, vol. 2, 2020, pp. 776–790 (cit. on pp. 4, 5).

[32] F. Krömer, F. Czwielong and S. Becker, “Experimental investigation of the sound emission of skewed axial fans with leading-edge serrations”, *Aiaa Journal*, vol. 57, no. 12, pp. 5182–5196, 2019 (cit. on pp. 4, 5, 17).

[33] C. Ocker, F. Czwielong, P. Chaitanya, W. Pannert and S. Becker, “Aerodynamic and aeroacoustic properties of axial fan blades with slitted leading edges”, *Acta Acustica*, vol. 6, p. 48, 2022 (cit. on pp. 4, 16).

[34] M. Piellard, B. B. Coutty, V. Le Goff, V. Vidal and F. Pérot, “Direct aeroacoustics simulation of automotive engine cooling fan system: Effect of upstream geometry on broadband noise”, in *20th AIAA/CEAS Aeroacoustics Conference*, 2014, p. 2455 (cit. on pp. 4, 5).

[35] S. Allam and M. Åbom, “Noise reduction for automotive radiator cooling fans”, *configurations*, vol. 15, p. 17, 2015 (cit. on pp. 4, 5).

[36] F. Czwielong, S. Floss, M. Kaltenbacher and S. Becker, “Influence of a micro-perforated duct absorber on sound emission and performance of axial fans”, *Applied Acoustics*, vol. 174, p. 107 746, 2021 (cit. on pp. 4, 5).

[37] M. Karlsson and S. Etemad, “Installation effects on the flow generated noise from automotive electrical cooling fans”, SAE Technical Paper, Tech. Rep., 2020 (cit. on pp. 4, 5).

[38] R. Guo, T. Mi, L. Li and R. Luo, "Research on aerodynamic performance and noise reduction of high-voltage fans on fuel cell vehicles", *Applied Acoustics*, vol. 186, p. 108 454, 2022 (cit. on p. 5).

[39] L. Feng, *Acoustical measurements* (Trita-AVE (Department of Aeronautical and Vehicle Engineering, Royal Institute of Technology), 2007:07), eng. Stockholm: KTH Engineering Sciences, 2007 (cit. on pp. 5, 9, 18).

[40] ISO Central Secretary, "ISO 3745:2012 Acoustics — Determination of sound power levels and sound energy levels of noise sources using sound pressure — Precision methods for anechoic rooms and hemi-anechoic rooms", en, International Organization for Standardization, Geneva, CH, Standard ISO 3745:2012, 2012. [Online]. Available: `https://www.iso.org/standard/45362.html` (cit. on pp. 5, 9, 10, 13, 14, 19).

[41] T. J. Mueller, *Aeroacoustic measurements*. Springer Science & Business Media, 2002 (cit. on pp. 5, 8–10, 16, 20, 30).

[42] S. V. Suárez, F. I. G. Colón, J. González *et al.*, "Evaluation of interaction and blockage effects for multi-fan units used in public transport hvac systems", *International Journal of Ventilation*, vol. 13, no. 4, pp. 339–350, 2015 (cit. on p. 5).

[43] A. Frid, M Abom, Y. Jiang, Y. Wang and K.-R. Fehse, "Cooling fans in railway vehicles-application of noise control measures to a roof-mounted engine cooler", *Fan Noise*, 2007 (cit. on p. 5).

[44] S. Heo, M. Ha, T.-H. Kim and C. Cheong, "Development of high-performance and low-noise axial-flow fan units in their local operating region", *Journal of Mechanical Science and Technology*, vol. 29, pp. 3653–3662, 2015 (cit. on p. 5).

[45] P. V. Gullberg, *Optimisation of the flow process in engine bays-3d modelling of cooling airflow*. Chalmers Tekniska Hogskola (Sweden), 2011 (cit. on p. 7).

[46] M. Vourakis and M. Karlsson, "Aeroacoustic interaction effects between parallel low-pressure axial flow fans", in *10th Convention of the European Acoustics Association, Forum Acusticum 2023*, Torino,Italy 10-15 Septeber 2023 (cit. on pp. 7, 17, 18, 21–23).

[47] M. Vourakis and M. Karlsson, "A round robin test of a low-pressure axial fan", *FAN 2022 International Conference on Fan Noise, Aerodynamics, Applications and Systems*, 10 Seiten, 2022. DOI: `https://doi.org/10.26083/tuprints-00021703` (cit. on pp. 8, 10).

[48] H.-P. Wallin, U. Carlsson, M. Åbom, H. Bodén, R. Glav and R. Hildebrand, *Sound and vibration*, eng, 2., rev. uppl. Stockholm: Institutionen för farkostteknik, Tekniska högskolan, 2010, ISBN: 978-91-7415-553-2 (cit. on pp. 8, 10–12).

[49] ISO Central Secretary, "ISO 3744:2010 Acoustics — Determination of sound power levels and sound energy levels of noise sources using sound pressure — Engineering methods for an essentially free field over a reflecting plane", en, International Organization for Standardization, Geneva, CH, Standard ISO 3744:2010, 2010. [Online]. Available: `https://www.iso.org/standard/45362.html` (cit. on pp. 9, 10, 13, 14, 19, 20, 25, 26, 29).

[50] M. Long, *Architectural acoustics*. Elsevier, 2005 (cit. on pp. 9, 10, 12).

[51] M. J. Crocker, *Handbook of noise and vibration control*. John Wiley & Sons, 2007 (cit. on pp. 9, 10, 12).

[52] J. Allen and D. Berkley, "Image method for efficiently simulating small-room acoustics", *The Journal of the Acoustical Society of America*, pp. 943–950, 1979. [Online]. Available: `http://scitation.aip.org/content/asa/journal/jasa/65/4/10.1121/1.382599` (cit. on pp. 10, 12).

[53] M. Åbom, *An introduction to flow acoustics*. Skolan för teknikvetenskap, Kungliga Tekniska högskolan, 2006 (cit. on p. 11).

[54] E. Skudrzyk, *The foundations of acoustics: basic mathematics and basic acoustics*. Springer Science & Business Media, 2012 (cit. on p. 14).

[55] B. Rafaely, Y. Peled, M. Agmon, D. Khaykin and E. Fisher, "Spherical microphone array beamforming", *Speech Processing in Modern Communication: Challenges and Perspectives*, pp. 281–305, 2010 (cit. on pp. 14, 15).

[56] M. Nolan, M. Berzborn and E. Fernandez-Grande, "Isotropy in decaying reverberant sound fields", *The Journal of the Acoustical Society of America*, vol. 148, no. 2, pp. 1077–1088, 2020 (cit. on pp. 14, 15).

[57] F. Zotter, A. Sontacchi, M. Noisternig and R. Höldrich, "Capturing the radiation characteristics of the bonang barung", in *Proc. of the 3rd AAAA Congress*, 2007, pp. 27–28 (cit. on p. 15).

[58] H. Pomberger, F. Zotter and A Sontacchi, "An ambisonics format for flexible playback layouts", in *Proc. 1st Ambisonics Symposium*, 2009, p. 8 (cit. on p. 15).

[59] R. Merino-Martínez, P. Sijtsma, M. Snellen *et al.*, "A review of acoustic imaging methods using phased microphone arrays: Part of the "aircraft noise generation and assessment" special issue", *CEAS Aeronautical Journal*, vol. 10, pp. 197–230, 2019 (cit. on p. 16).

[60] G. Herold and E. Sarradj, "Microphone array method for the characterization of rotating sound sources in axial fans", *Noise Control Engineering Journal*, vol. 63, no. 6, pp. 546–551, 2015 (cit. on p. 16).

[61] F. J. Krömer, S. Moreau and S. Becker, "Experimental investigation of the interplay between the sound field and the flow field in skewed low-pressure axial fans", *Journal of Sound and Vibration*, vol. 442, pp. 220–236, 2019 (cit. on p. 16).

[62] T. Benedek and J. Vad, “An industrial onsite methodology for combined acoustic-aerodynamic diagnostics of axial fans, involving the phased array microphone technique”, *International Journal of Aeroacoustics*, vol. 15, no. 1-2, pp. 81–102, 2016 (cit. on p. 16).

[63] T. Benedek, J. Vad and B. Lendvai, “Combined acoustic and aerodynamic investigation of the effect of inlet geometry on tip leakage flow noise of free-inlet free-exhaust low-speed axial flow fans”, *Applied Acoustics*, vol. 187, p. 108 488, 2022 (cit. on p. 16).

[64] H.-E. Albrecht, N. Damaschke, M. Borys and C. Tropea, *Laser Doppler and phase Doppler measurement techniques*. Springer Science & Business Media, 2013 (cit. on pp. 17, 21–23).

[65] Z. Zhang, *LDA application methods: laser Doppler anemometry for fluid dynamics*. Springer Science & Business Media, 2010 (cit. on pp. 17, 20–23).

[66] R. Franzke, *Experimental and numerical investigations of underhood flow for vehicle thermal management*. Chalmers Tekniska Hogskola (Sweden), 2021 (cit. on p. 17).

[67] D. Ragni, *EAA Summer school 2023,lecture notes: Advanced non-intrusive techniques for aeroacosutics*, 2023 (cit. on p. 18).

[68] M. Handbook, “Technical documentation”, *Brüel&Kjaer, Naerum*, 2019 (cit. on p. 18).

[69] *Signals and Mechanical Systems,Lecture notes,KTH Royal Institute of Technology*, 2018 (cit. on p. 19).

[70] T. Arts, H. Boerrigter, M. Carbonaro *et al.*, “Measurement techniques in fluid dynamics. an introduction, von karman institute for fluid dynamics”, *Rhode-Saint-Genese*, pp. 43–274, Jan. 2001 (cit. on pp. 20, 21).

[71] *LDA and PDA Reference Manual,Dantec Dynamics*, 2011 (cit. on pp. 21, 22).

[72] F. Zenger, C. Junger, M. Kaltenbacher and S. Becker, “A benchmark case for aerodynamics and aeroacoustics of a low pressure axial fan”, SAE Technical Paper, Tech. Rep., 2016 (cit. on pp. 25, 26).